Available online at www.sciencedirect.com
SCIENCE DIRECT®
ELSEVIER
Journal of Non-Crystalline Solids 326&327 (2003) 146–153
JOURNAL OF NON-CRYSTALLINE SOLIDS
www.elsevier.com/locate/jnoncrysol

Thermal relaxation of the structural and optical properties of amorphous $As_{40}S_{60-x}Se_x$ films

J.M. González-Leal [a,*], Mir. Vlček [b], R. Prieto-Alcón [c], A. Stronski [d], T. Wágner [b], E. Márquez [c]

[a] Department of Chemistry, University of Cambridge, Lensfield Road, CB2 1EW, Cambridge, UK
[b] Department of General and Inorganic Chemistry, University of Pardubice, 53210 Pardubice, Czech Republic
[c] Departamento de Física de la Materia Condensada, Facultad de Ciencias, Universidad de Cádiz, 11510 Puerto Real (Cádiz), Spain
[d] Institute of Semiconductor Physics, NAS, Prospect Nauki 45, 252028 Kiev-28, Ukraine

Abstract

This paper deals with the structural and optical properties of virgin (i.e., as-evaporated) and annealed (i.e., thermally relaxed) amorphous $As_{40}S_{60-x}Se_x$ films ($x = 0$, 20, 30, 40 and 60 at.%), which were prepared by vacuum evaporation. Structural properties have been inferred from the X-ray diffraction patterns and the Raman spectra of the thin-film samples. The decrease in the intensity of the first sharp diffraction peak after annealing suggests that the thermal relaxation is connected with a decrease in the free volume leading to an increase of the structural compactness. A significant decrease in film thickness has been invariably found after annealing in all cases, which supports this conclusion. Changes found in the Raman spectra of the film samples after annealing indicate a reduction in the concentration of homopolar bonds, which are present in the molecular fragments embedded in the amorphous matrix. Thus, the thermodynamic state of the system is shifted towards equilibrium as a result of thermally induced polymerization (homogenization). These structural changes also resulted in significant changes in both the refractive index and optical band gap, E_g^{opt}.

PACS: 81.40.−z; 78.30.Ly; 78.70.Ck; 78.66.Jg

1. Introduction

Physical properties of amorphous solids are strongly modified by thermally induced structural relaxation occurring during the time [1–6]. From a technological application point of view, this aging effect must be considered to restrict the operating life of the devices made from these materials [7–11].

The aim of this paper is to analyze the changes in both the structural and optical properties of amorphous $As_{40}S_{60-x}Se_x$ films ($x = 0$, 20, 30, 40 and 60 at.%) prepared by vacuum evaporation, as a consequence of the thermally induced structural relaxation. This aging effect was simulated by annealing at temperatures near the glass-transition

* Corresponding author. Tel.: +44-1223 3 36532; fax: +44-1223 3 36362.
E-mail address: jmg62@cam.ac.uk (J.M. González-Leal).

0022-3093/$ - see front matter © 2003 Elsevier B.V. All rights reserved.
doi:10.1016/S0022-3093(03)00394-6

temperature, T_g, samples of a given composition. Structural properties have been inferred from both X-ray diffraction (XRD) patterns and Raman spectra of the thin-film samples. Optical properties have been derived from the transmission spectra, taken at normal incidence, in the spectral range 400–2200 nm. A detailed analysis of the compositional dependencies of the optical properties of the as-evaporated amorphous $As_{40}S_{60-x}Se_x$ films can be found in Ref. [12].

2. Experimental

Amorphous $As_{40}S_{60-x}Se_x$ films ($x = 0$, 20, 30, 40 and 60 at.%) were prepared according to the procedure described in Ref. [12]. Actual chemical compositions of the chalcogenide films were found to be $As_{38.7\pm0.8}S_{61.6\pm0.7}$, $As_{39.8\pm0.5}S_{39.9\pm0.6}Se_{20.3\pm0.3}$, $As_{38.9\pm1.4}S_{31.0\pm0.5}Se_{30.2\pm1.7}$, $As_{39.1\pm1.9}S_{22.2\pm0.9}Se_{38.7\pm1.9}$ and $As_{41.2\pm1.8}Se_{58.8\pm1.8}$, on the basis of electron microprobe X-ray analysis, using a scanning electron microscope (JEOL, model JSM-820). The lack of crystallinity in the films was systematically verified by XRD measurements (Philips, model PW-1820). Annealing of the as-deposited samples was performed in vacuum at 160 °C during 24 h, which is well below the glass-transition temperature of these compositions: $T_g \geqslant 180$ °C, increasing with Se content [13]. Mass measurements were made by a microbalance (Mettler, model AE200) to check possible changes after annealing.

The Raman spectra were measured by using a Fourier Transform IR spectrometer (Bruker, model IFS 55) with a Raman accessory (Bruker, model FRA 106). Laser irradiation at the wavelength of 1064 nm (1.16 eV), coming from a Nd-YAG laser, was used for the excitation of the Raman spectra. Such a low energy was suitable for our experiments as it is well below the values of the optical band gaps for the glassy alloys under study (1.75 eV and greater, see Table 1 from Results). Thus, no detectable photostructural transformation took place during the data collection (200 scans, laser output power 90 mW), and spectra with a resolution of 1 cm^{-1} were successfully measured even for virgin (as-evaporated) films. The optical transmission spectra were obtained at

Table 1
Geometrical and optical parameters for the virgin (v) and annealed (a) amorphous $As_{40}S_{60-x}Se_x$ films studied

x (at.%)	Status	$\bar{d}$ (nm)	$\Delta\bar{d}$ (nm)	Δ (nm)	E_o (eV)	ΔE_o (eV)	E_d (eV)	ΔE_d (eV)	N_c	$n(0)$	$\Delta n(0)$	E_g^{opt} (eV)	ΔE_g^{opt} (eV)
0	v	1098 ± 4	−60 ± 10	9 ± 1	4.94 ± 0.03	−0.13 ± 0.05	20.67 ± 0.12	+1.16 ± 0.21	3.0 ± 0.3	2.277 ± 0.001	+0.076 ± 0.002	2.43 ± 0.01	−0.05 ± 0.02
	a	1038 ± 6	(−5.5%)	10 ± 1	4.81 ± 0.02		21.83 ± 0.09		3.2 ± 0.3	2.353 ± 0.001	(+3.3%)	2.38 ± 0.01	
20	v	1148 ± 5	−54 ± 10	14 ± 1	4.53 ± 0.03	−0.23 ± 0.05	21.64 ± 0.14	+0.82 ± 0.24	3.1 ± 0.3	2.404 ± 0.001	+0.090 ± 0.002	2.13 ± 0.01	−0.04 ± 0.02
	a	1094 ± 5	(−4.7%)	15 ± 1	4.30 ± 0.02		22.46 ± 0.10		3.2 ± 0.3	2.494 ± 0.001	(+3.7%)	2.09 ± 0.01	
30	v	914 ± 3	−19 ± 7	8 ± 1	4.31 ± 0.04	−0.33 ± 0.06	21.65 ± 0.20	+0.77 ± 0.34	3.1 ± 0.3	2.454 ± 0.001	+0.121 ± 0.003	2.01 ± 0.01	−0.04 ± 0.02
	a	895 ± 4	(−2.1%)	11 ± 1	3.98 ± 0.02		22.42 ± 0.14		3.2 ± 0.3	2.575 ± 0.002	(+4.9%)	1.97 ± 0.01	
40	v	769 ± 3	−45 ± 5	8 ± 1	4.18 ± 0.02	−0.30 ± 0.05	22.54 ± 0.13	+0.81 ± 0.29	3.3 ± 0.3	2.528 ± 0.001	+0.121 ± 0.003	1.94 ± 0.01	−0.05 ± 0.02
	a	724 ± 2	(−5.9%)	9 ± 1	3.88 ± 0.03		23.35 ± 0.16		3.4 ± 0.3	2.649 ± 0.002	(+4.8%)	1.89 ± 0.01	
60	v	939 ± 5	−22 ± 9	–	3.86 ± 0.02	−0.20 ± 0.05	23.74 ± 0.11	+0.54 ± 0.29	3.4 ± 0.3	2.674 ± 0.001	+0.089 ± 0.003	1.79 ± 0.01	−0.04 ± 0.02
	a	917 ± 4	(−2.3%)	–	3.66 ± 0.03		24.28 ± 0.18		3.5 ± 0.3	2.763 ± 0.002	(+3.3%)	1.75 ± 0.01	

normal incidence by a double-beam spectrophotometer (Perkin–Elmer, model Lambda-19), which covers the spectral range ultraviolet/visible/near-infrared (UV/Vis/NIR). The wavelength range analyzed was between 400 and 2200 nm. A surface-profiling stylus (Sloan, model Dektak 3030) was used to measure independently the film thicknesses, which were compared with those calculated from the transmission spectra.

Thin-film samples were kept in complete darkness until measured in order to minimize exposure to light sources, which could lead to changes in the optical properties and possible oxidation of the films [14]. Experiments were carried out two months after the preparation of the films. All measurements were performed at room temperature.

3. Results

3.1. X-ray diffraction

Fig. 1 shows the XRD patterns corresponding to as-deposited and annealed amorphous $As_{40}S_{60-x}Se_x$ films. Besides illustrating the amorphous nature of the samples, the XRD patterns for the virgin films also show the so-called first sharp diffraction peak (FSDP), which occurs at values of the scattering vector $Q(=4\pi\sin\theta/\lambda) = 1$–$2$ Å^{-1}, depending on the material [15,16]. This feature has been traditionally associated with the presence of medium-range order (MRO) in amorphous materials, and many attempts have been made to explain its origin. Among the various models suggested, that proposed by Elliott [17,18] should be highlighted. According to this author, the FSDP is ascribed to the presence of interstitial volume around the cation-centered structural units or, in other words, to an *ordered* pattern of voids in the amorphous matrix, which characterizes the MRO in the non-crystalline solid.

It is observed from Fig. 1 that the intensity of the FSDP decreases non-monotonically with increasing Se content, reaching a minimum around intermediate ternary compositions. It can also be seen that after annealing of the virgin samples, the intensity profile of the FSDP strongly decreases in all cases, which indicates notable thermally

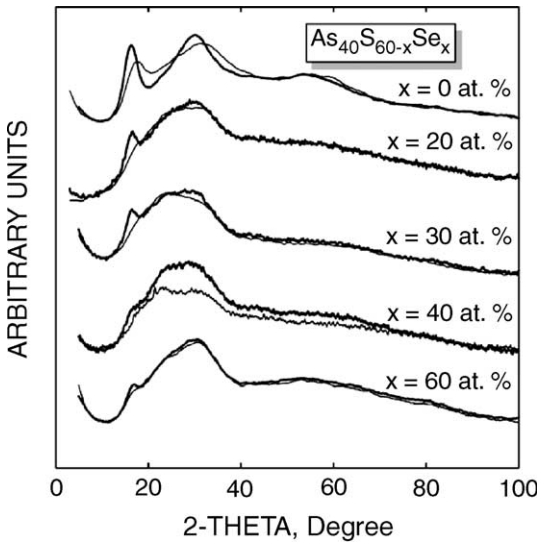

Fig. 1. XRD patterns for the as-evaporated (thick lines) and annealed (thin lines) amorphous $As_{40}S_{60-x}Se_x$ films.

induced structural changes. In addition, a shift of this XRD feature to higher angles after annealing, can be clearly observed in the particular case of the amorphous $As_{40}S_{60}$ film. A similar behavior was reported by De Neufville et al. [1] for thermally evaporated As_2S_3 and As_2Se_3 films. XRD patterns of the annealed samples for the rest of the compositions studied show a quasi-disappearance of the FSDP. Therefore, it is certainly difficult to express some comment about any shift of this feature with respect to the virgin case. These changes found in the XRD patterns suggest, following Elliott's ideas, a diminution of the interstitial volume around the structural units forming the amorphous network of the $As_{40}S_{60-x}Se_x$ layers or, in other words, a thermal densification of the films (changes in the masses of the samples were not found after annealing).

3.2. Raman spectroscopy

The Raman spectra of as-evaporated and annealed films of two different intermediate ternary compositions within the composition line under study, namely, $As_{40}S_{40}Se_{20}$ and $As_{40}S_{20}Se_{40}$, are compared with the Raman spectra of bulk samples of the same compositions in Fig. 2. A good

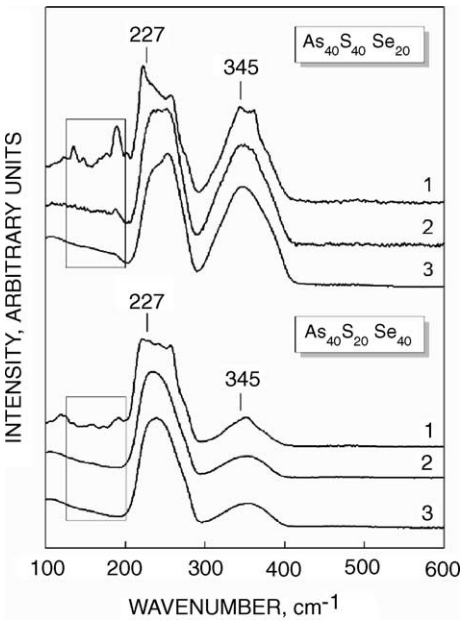

Fig. 2. Raman spectra of $As_{40}S_{40}Se_{20}$ and $As_{40}S_{20}Se_{40}$ samples: (1) virgin film, (2) film after annealing in vacuum at 160 °C for 24 h, and (3) bulk glass. Spectra have been normalized by area and shifted vertically for the sake of clarity. Boxes have been drawn to highlight the differences between the spectra at low wavenumbers.

correlation between the position of the main bands in the Raman spectra of bulk samples, virgin and annealed films exists. Thus, one can conclude that the same basic structural units form the glass matrix of a given composition. The main broad bands (regions 220–260 and 320–380 cm^{-1}) are *structured*, i.e., they are in fact, the result of the overlapping of narrower bands. At the same time, it is observed that some additional weaker bands exist in the Raman spectra of virgin films (mainly in the region 125–200 cm^{-1}). These differences between the spectra of virgin films and bulk glasses become more significant as the S content in the $As_{40}S_{60-x}Se_x$ samples increases – differences are not so notable in the case of annealed samples.

3.3. UV/Vis/NIR spectroscopy

Both as-evaporated and annealed amorphous $As_{40}S_{60-x}Se_x$ films, have been geometrically and optically characterized from their corresponding optical transmission spectra, $T(\lambda)$, taken at normal incidence. Improved analytical expressions for the envelopes of the transmission spectra (both for uniform and non-uniform films in thickness), which take into account the weak absorption in the substrate [19], were implemented into the well-known envelope characterization method [20,21]. This new approach has allowed us to determine the average thickness of the films, $\bar{d}$, and the refractive index, n, with accuracies better than 1%. It is worth noting that, even though a planetary rotary system was used in order to reduce to some extent the non-uniformity in the thickness of the films [12], most of the samples showed an appreciable lack of uniformity in thickness, the only exception being the $As_{40}Se_{60}$ films. Values of the thickness variation, Δ, at the extreme of the spectrophotometer light spot area (1×4 mm^2) are listed in Table 1. All the details about the formulation and the algorithm used for the determination of the above-mentioned geometrical and optical parameters can be found in Ref. [19].

Spectral dependencies of the refractive index, $n(\lambda)$, for the as-evaporated and annealed amorphous $As_{40}S_{60-x}Se_x$ films studied are plotted in Fig. 3. The dispersion of the refractive index has been analyzed on the basis of the Wemple–Di-Domenico (WDD) model [22,23], which is based on the single-oscillator formula

$$n^2(\hbar\omega) = 1 + \frac{E_o E_d}{E_o^2 - (\hbar\omega)^2}, \tag{1}$$

where E_o is the single-oscillator energy and E_d the dispersion energy or single-oscillator strength. An important achievement of the WDD model is that it relates the dispersion energy, E_d to other physical parameters of the material through the following empirical relationship [22,23]:

$$E_d = \beta N_c Z_a N_e \quad (\text{eV}), \tag{2}$$

where N_c is the effective coordination number of the cation nearest-neighbour to the anion, Z_a is the formal chemical valency of the anion, N_e is the effective number of valence electrons per anion, and β is a two-valued constant with either an ionic or a covalent value ($\beta_i = 0.26 \pm 0.03$ eV and $\beta_c = 0.37 \pm 0.04$ eV, respectively).

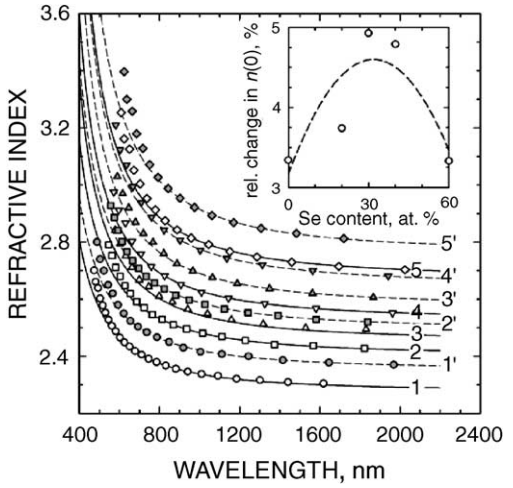

Fig. 3. Refractive-index dispersion of the amorphous $As_{40}S_{60-x}Se_x$ films obtained from their transmission spectra. Plots correspond to the following compositions: (1) $As_{40}S_{60}$, (2) $As_{40}S_{40}Se_{20}$, (3) $As_{40}S_{30}Se_{30}$, (4) $As_{40}S_{20}Se_{40}$, and (5) $As_{40}Se_{60}$. The superscript prime indicates annealed samples. Curves have been drawn according to Eq. (1). Relative changes in the static refractive index, $n(0)$, are plotted in the inset as a function of the Se content. The dashed line is a guide for the eye.

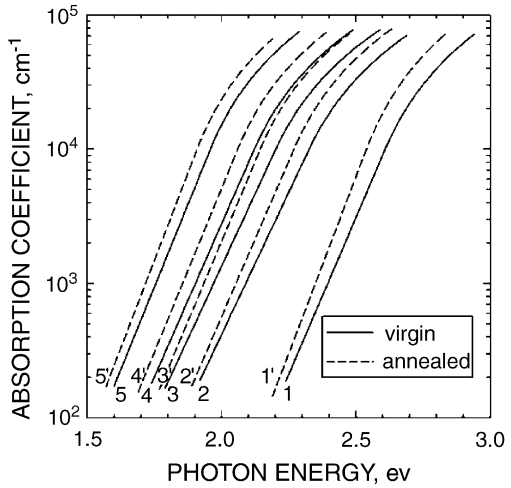

Fig. 4. Spectral dependencies of the absorption coefficient, $\alpha(\hbar\omega)$, for the amorphous $As_{40}S_{60-x}Se_x$ films. Plots correspond to the following compositions: (1) $As_{40}S_{60}$, (2) $As_{40}S_{40}Se_{20}$, (3) $As_{40}S_{30}Se_{30}$, (4) $As_{40}S_{20}Se_{40}$, and (5) $As_{40}Se_{60}$. The superscript prime indicates annealed samples.

On the other hand, the optical absorption spectra, $\alpha(\hbar\omega)$, for the virgin and annealed amorphous $As_{40}S_{60-x}Se_x$ films under study, are displayed in Fig. 4 using a semi-logarithmic scale. Details about the formulation and the algorithm used for the calculation of $\alpha(\hbar\omega)$ can also be found in Ref. [19]. A systematic red shift of the optical absorption edge is observed in all cases after annealing (i.e., thermal darkening), which indicates a decrease in the optical band gap. Analysis of the strong absorption region ($\alpha \gtrsim 10^4$ cm^{-1}) has been carried out using the following well-known quadratic equation, which is often called the Tauc law [24]:

$$\alpha(\hbar\omega) = B\frac{(\hbar\omega - E_g^{opt})^2}{\hbar\omega}, \qquad (3)$$

where B is a constant, which depends on the electronic transition probability, and E_g^{opt} is the so-called Tauc gap. The values of E_g^{opt} for the as-evaporated and annealed amorphous $As_{40}S_{60-x}Se_x$ films have been derived by plotting $(\alpha\hbar\omega)^{1/2}$ versus $\hbar\omega$ (also called a Tauc plot), and they are all listed in Table 1. Finally, it is worth mentioning that the above-introduced single-oscillator energy E_o is considered as an 'average' energy gap and, to a good approximation, it varies in proportion to the Tauc gap, E_g^{opt}, according to the relationship $E_o \approx 2 \times E_g^{opt}$ [25].

Values for the average thickness, $\bar{d}$, the wedging parameter accounting for the non-uniform thickness of the films, Δ, the single-oscillator energy, E_o, the dispersion energy, E_d, the *static* refractive index, $n(0)$, which is determined by extrapolating Eq. (1) when $\hbar\omega \to 0$, as well as the Tauc gap, E_g^{opt}, corresponding to the virgin and thermally relaxed amorphous chalcogenide films under study, are all listed in Table 1. Absolute and relative values of the thermally induced changes of given parameters are also collected in Table 1.

4. Discussion

As mentioned above, XRD patterns corresponding to as-evaporated amorphous $As_{40}S_{60-x}Se_x$ films, which are plotted in Fig. 1, show a clear decrease in the intensity of the FSDP, as well as a shift to higher angles with increasing x. It has been

also pointed out that such a decrease does not scale with the Se content and a minimum in the intensity appears at intermediate values of x. This compositional dependence for the FSDP suggests a lower MRO for ternary compositions at the middle of the composition line and, according to Elliott's model [18], a lower concentration of interstitial voids for these intermediate compositions.

It can also be observed in Fig. 1 that the intensity profile of the FSDP decreases after annealing. It is well known [2,14,15,26] that thermally evaporated binary amorphous As–S and As–Se films often contain some of the molecular species of which the vapor is composed, e.g., $As_4S(Se)_4$, $As_4S(Se)_3$ and $S(Se)_n$. These kind of molecular clusters have been also reported in the case of ternary As–S–Se glassy alloys [13]. They make difficult the cohesion between the structural layers and increase the free volume in the material. These molecular species are unstable with respect to annealing. Their concentration is greatly reduced by polymerization and cross-linking with the amorphous network. As a consequence, a more effective interaction between the structural layers, through an increased number of intermolecular chemical bonds involving neighbouring structural layers, is achieved; the structure and mass density of the thermally relaxed chalcogenide film becomes closely identical to that of the corresponding bulk glass [15,16]. Thermal relaxation therefore leads to a compaction (densification) of the amorphous structure, i.e., a clear diminution of the interstitial volume around the $AsS_{3-n}Se_n$ ($n = 0, 1, 2, 3$) pyramidal structural units, which form the layered network of the $As_{40}S_{60-x}Se_x$ glasses [13,27]. The significant decrease in film thickness, which has been invariably found in all cases after annealing (see Table 1), supports this conclusion. It should be pointed out that thermal relaxation experiments recently reported by Malek [28] for $As_{40}S_{60}$ bulk glasses at 160.9 °C for 24 h, after a previous cooling from T_g led to a decrease in sample thickness of about 0.2%. This value differs by a factor of about 30 compared with the value found for the amorphous film with the same composition, 5.5%. Such a large difference between these values shows the high non-equilibrium state of the virgin amorphous chalcogenide films.

As mentioned earlier, the main bands of the Raman spectra of the $As_{40}S_{60-x}Se_x$ bulk glasses, virgin and annealed films appear in the same spectral regions. Bulk glasses of the binary compositions $As_{40}Se_{60}$ and $As_{40}S_{60}$ show quite *simple* Raman spectra with main bands at, respectively, 227 and 345 cm^{-1}, which are associated with vibrations of $AsSe_3$ and AsS_3 pyramidal units. As expected, bulk glasses of the ternary compositions show two main bands with maxima at frequencies close to the above-mentioned ones (see Fig. 2). Such a structure with two main bands is also preserved in the case of the thin films. Nevertheless, a number of additional features can also be observed in the spectra corresponding to the thin-film samples. Weak and narrow bands appearing in the region 125–200 cm^{-1} are associated to the presence of the above-introduced molecular fragments of the type $As_4S(Se)_4$, $As_4S(Se)_3$ and $S(Se)_n$, [11,13]. The concentration of these molecular species containing homopolar bonds is mainly evident in the spectra of the samples with high S content. Annealing results in all cases in a decrease in the intensity of these bands, which also supports the thermally induced polymerization of such molecular fragments.

Fig. 3 shows the dispersion of the refractive index, $n(\lambda)$, for the virgin and annealed amorphous $As_{40}S_{60-x}Se_x$ films. In all compositions, an increase in the values of the refractive index is observed with annealing, over the whole spectral region under study. In principle, this result could be related to the structural densification inferred from the XRD experiments, on the basis of the Lorentz–Lorenz relationship [29]

$$\frac{n^2-1}{n^2+2} = \frac{1}{3\varepsilon_0}\sum_j N_j \alpha_{p,j}, \tag{4}$$

where ε_0 is the vacuum permittivity and N_j the number of polarizable units of type j per volume unit, with polarizability $\alpha_{p,j}$. Thus, the increase in the concentration of polarizable units, N_j, after annealing (due to the thermally induced volume contraction), would lead to an increase in the refractive index. Eq. (4) can be rewritten as follows (neglecting possible changes in the polarizabilities), in order to show the relationship between the

changes in n and in the mass density, ρ (or equivalently, the average film thickness, $\bar{d}$):

$$\frac{\Delta n}{n} = \frac{6n^2}{(n^2-1)(n^2+2)}\frac{\Delta\rho}{\rho} = -\frac{6n^2}{(n^2-1)(n^2+2)}\frac{\Delta\bar{d}}{\bar{d}}. \quad (5)$$

Nevertheless, the relative changes found in the average thickness after annealing (see Table 1) do not account completely for the corresponding increases in the refractive index. In particular, for the changes in the static refractive index, $n(0)$ (see the inset of Fig. 3), the values of the mathematical expression on the right of Eq. (5) for all compositions studied were, respectively, 5.7%, 4.4%, 1.9%, 5.0% and 1.8%. The differences between the experimentally-obtained relative changes for $n(0)$ and those derived from Eq. (5) suggest that, apart from densification, notable changes in the effective polarizability of the material occur as a consequence of the rearrangement of the bonds. This hypothesis is consistent with the greater concentration of heteropolar bonds in the thermally relaxed samples, at the expense of the homopolar bonds forming the molecular clusters.

The increase observed in the dispersion energy, E_d, also supports the conclusion about the polymerization and the higher structural compactness of the films after annealing. Hence, an increase in the As effective coordination number can be inferred from Eq. (2). The thermally induced increase in the structural compactness would increase the interactions between structural layers through As atoms acting as bonding points, forming As$\cdots$Ch intermolecular bonds (Ch being a chalcogen atom), which would contribute to increase N_c (see Table 1).

Finally, a red shift of the optical absorption edge has been invariably found after annealing (see Fig. 4), which leads to darkening of the samples, as well as a decrease in the Tauc gap, E_g^{opt}. In a similar way, a decrease in the single-oscillator energy, E_o, from the WDD model has been found, as expected on the basis of the relationship $E_o \approx 2 \times E_g^{opt}$. This behavior is consistent with the significant decrease in the concentration of homopolar bonds of the type As–As (in the molecular species $As_4S(Se)_4$ and $As_4S(Se)_3$, for instance), S–S (in S_n rings or chains) and Se–Se (in Se_n rings or chains), leading to an also significant increase in the concentration of heteropolar bonds of the type As–S and As–Se, with lower bonding energies (379.5 and 96 kJ/mol, respectively) than the homopolar ones (As–As, 382.0 kJ/mol; S–S, 425.3 kJ/mol; Se–Se, 332.6 kJ/mol).

5. Conclusions

Structural properties of virgin and thermally relaxed amorphous $As_{40}S_{60-x}Se_x$ films ($x = 0$, 20, 30, 40 and 60 at.%), have been derived from their XRD patterns and Raman spectra. Both techniques support the idea that thermally induced structural relaxation is linked to the polymerization of molecular fragments embedded in the structure of the as-evaporated films. Changes observed in the optical properties of these amorphous films are consistent with the structural changes inferred.

Acknowledgements

The authors are grateful to Professor S.R. Elliott (Department of Chemistry, University of Cambridge, UK) for a critical reading of the paper. This work has been partly supported by a Marie Curie Fellowship of the European Community programme 'Improving Human Research Potential and the Socio-Economic Knowledge Base' under contract number HPMF-CT-2000-01031, and by the MCYT (Spain) and FEDER (CEE) under MAT2001-3333 research project.

References

[1] J.P. De Neufville, S.C. Moss, S.R. Ovshinsky, J. Non-Cryst. Solids 13 (1973&74) 191.
[2] S.A. Solin, G.N. Papatheodorou, Phys. Rev. B 15 (1977) 2084.
[3] S. Etienne, J.Y. Cavaille, J. Perez, G.P. Johari, Philos. Mag. A 51 (1985) L35.
[4] D. Tonchev, S.O. Kasap, Mater. Sci. Eng. A-Struct. 328 (2002) 62.

[5] O.S. Naraynaswamy, J. Am. Ceram. Soc. 54 (1971) 491.
[6] G.W. Scherer, Relaxation in Glass and Composites, Wiley–Interscience, New York, 1986.
[7] T. Todorov, L. Nikolova, K. Stoyanova, N. Tomava, Appl. Opt. 24 (1985) 785.
[8] C.H. Kwak, J.T. Kim, S.S. Lee, Appl. Opt. 28 (1989) 737.
[9] A.V. Stronski, M. Vlcek, A. Sklenar, P.E. Shepeljavi, S.A. Kostyukevich, T. Wagner, J. Non-Cryst. Solids 266–269 (2000) 973.
[10] N. Nordman, O. Nordman, Opt. Eng. 40 (2001) 2572.
[11] A.V. Stronski, M. Vlcek, J. Opt. Adv. Mater. 4 (2002) 699.
[12] J.M. González-Leal, R. Prieto-Alcón, J.A. Angel, E. Márquez, J. Non-Cryst. Solids 315 (2003) 134.
[13] M. Vlcek, A.V. Stronski, A. Sklenar, T. Wagner, S.O. Kasap, J. Non-Cryst. Solids 266–269 (2000) 964.
[14] J.S. Berkes, S.W. Ing Jr., W.J. Hillegas, J. Appl. Phys. 42 (1971) 4908.
[15] S.R. Elliott, Physics of Amorphous Materials, 2nd Ed., Longman, London, 1990.
[16] S.R. Elliott, in: J. Zarzycki (Ed.), Materials Science and Technology, vol. 9, VCH, Weinheim, 1991, p. 375.
[17] S.R. Elliott, Nature 354 (1991) 445.
[18] S.R. Elliott, Phys. Rev. Lett. 67 (1991) 711.
[19] J.M. González-Leal, R. Prieto-Alcón, J.A. Angel, D.A. Minkov, E. Márquez, Appl. Opt. 41 (2002) 7300.
[20] R. Swanepoel, J. Phys. E: Sci. Instrum. 16 (1983) 1214.
[21] R. Swanepoel, J. Phys. E: Sci. Instrum. 17 (1984) 896.
[22] S.H. Wemple, M. DiDomenico, Phys. Rev. B 3 (1971) 1338.
[23] S.H. Wemple, Phys. Rev. B 7 (1973) 3767.
[24] J. Tauc, in: J. Tauc (Ed.), Amorphous and Liquid Semiconductors, Plenum, New York, 1974, p. 159.
[25] Ke. Tanaka, Thin Solid Films 66 (1980) 271.
[26] A.V. Kolobov, Ka. Tanaka, in: Hari Singh Nalwa (Ed.), Handbook of Advanced Electronic and Photonic Materials and Devices, vol. 5, Academic Press, San Diego, CA, 2001, p. 47.
[27] J.A. Freitas, U. Strom, D.J. Treacy, J. Non-Cryst. Solids 59&60 (1983) 875.
[28] J. Malek, Thermochim. Acta 311 (1998) 183.
[29] S.R. Elliott, The Physics and Chemistry of Solids, Wiley, Chichester, 2000.